

We are IntechOpen, the world's leading publisher of Open Access books Built by scientists, for scientists

6,900

Open access books available

186,000

International authors and editors

200M

Downloads

Our authors are among the

154

Countries delivered to

TOP 1%

most cited scientists

12.2%

Contributors from top 500 universities



WEB OF SCIENCE™

Selection of our books indexed in the Book Citation Index
in Web of Science™ Core Collection (BKCI)

Interested in publishing with us?
Contact book.department@intechopen.com

Numbers displayed above are based on latest data collected.
For more information visit www.intechopen.com



Brushless Electric Machines with Axial Magnetic Flux: Analysis and Synthesis

Sergey Gandzha and Dmitry Gandzha

Abstract

An analysis of electric machines with axial magnetic flux is given. First, the effect of commutation on the electromagnetic moment and electromagnetic power is analyzed. Two types of discrete switching are considered. The analysis is performed for an arbitrary number of phases. The first type of switching involves disabling one phase for the duration of switching. The second type of switching involves the operation of all phases in the switching interval. The influence of the pole arc and the number of phases on the electromagnetic moment and electromagnetic power is investigated. The conclusion is made about the advantage of the second type of switching. It is recommended to increase the number of phases. Next, the classification of the main structures of the axial machine is carried out. Four main versions are defined. For each variant, the equation of the electromagnetic moment and electromagnetic power is derived. This takes into account the type of commutation. The efficiency of the selected structures is analyzed. The comparative analysis is tabulated for choosing the best option. The table is convenient for engineering practice. This chapter forms the basis for computer-aided design of this class of machines.

Keywords: brushless electric machine, axial gap electric machine, discrete commutation, multiphase electric machine, electromagnetic moment, electromagnetic power, permanent magnet, cylindrical magnet, segment magnet, diamagnetic anchor

1. Introduction

Low- and medium-power electric drives based on brushless electric machines are widely used both in industrial applications and in special-purpose products (space, medicine, robotics). Traditionally, brushless electric machines with a radial magnetic flux are used for this purpose. This is due to the good specific energy indicators of these electric machines, well-established technology of their production [1–7].

Recently, brushless electric machines with axial magnetic flux (BMAMF) have been increasingly used for these purposes. These electric machines are actively developing, and we can talk about the formation of a new class of brushless electric drives that are competitive with traditional brushless electric drives. There is a process of transition from the design of individual products to the development of an industrial range of electric machines of this type. International and domestic practice confirms this trend [8–12].

The following reasons can explain the active introduction of electric machines of this class into production:

- at present, the industrial production of powerful magnets with high values of residual induction and coercive force has been intensively developed, which allowed to concentrate the energy of the magnetic field in small volumes and reduce the size of electric machines;
- modern development of computing tools and special software allows you to optimize the geometry of BMAMF for efficient use of the volume occupied by them. At the same time, optimally designed BMAMF under conditions of limited size can have better specific weight size and energy indicators compared to radial electric machines;
- modern technologies allow to create BMAMF more economical to manufacture and reliable in operation.

It should be noted that, despite the urgent need for practical implementation, theoretical research on the analysis and synthesis of electric machines of this class is episodic and scattered. As a rule, developers analyze one design for a special drive. The results of these studies are quite difficult to transform into another constructive type. The influence of the electronic switch on the engine characteristics has not been fully studied.

Recently, there has been a tendency to increase the number of phases to improve reliability [13]. At the same time, the switching theory for multiphase BMAMF execution is not sufficiently covered in scientific publications and requires further improvement and development.

There is no unified theory for calculating electric machines of this class that would link electromagnetic power with electromagnetic loads and basic dimensions, taking into account design features.

Thus, the existing contradiction between the practical need for implementation and the insufficiently developed theory of analysis and synthesis is the main source of further development of electric machines of this class, which determines the relevance of scientific research in this area.

2. Analysis of the effect of commutation on the electromagnetic moment for any number of phases of the anchor winding for BMAMF

The winding of the brushless electric machine is connected to the power source via a commutator. Its principle of operation is as follows: when the rotor is turned, those sections of the armature winding are connected to the source, which are most profitable to pass current through from the point of view of creating an electromagnetic moment.

Switching the valve machine should be understood as connecting and disconnecting the phases of the armature winding with electronic keys to the power source. The main characteristics of the electric machine depend on the choice of switching method: moment, power consumption and useful power, efficiency, current.

The classification of the main types of switching of brushless machines is shown in **Figure 1**. Analog switching implements vector control of the brushless machine. Vector control is a control method that generates harmonic phase currents and controls the magnetic flux of the rotor. Currently, vector control systems are well developed in theory and implemented in practice. They have a wide range of applications, due to the development of power electronics, which allows you to create reliable and relatively cheap converters, as well as the development of high-speed

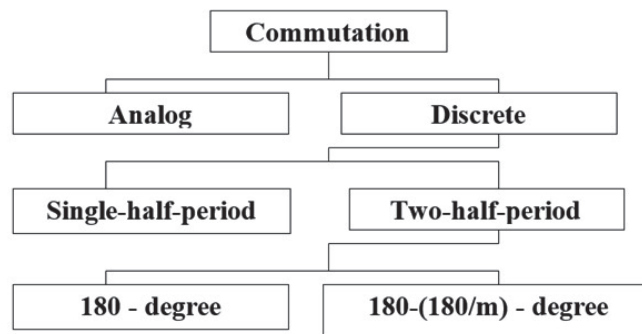


Figure 1.
The classification of the main types of switching of BMAMF.

microelectronics that can implement control algorithms of almost any complexity. However, it is necessary to recognize the great complexity of implementing this type of switching. For this reason, it is not considered in the work.

In contrast to analog switching, in discrete switching, electronic keys on the inter-switching interval have only two States: on and off. Discrete switching by the nature of the current is divided into one-half-period switching, when the current in the phase sections flows in only one direction, and two-half-period switching, when the current flows in both directions.

Single-half-period switching is simple enough to implement, since it requires only one key per switched phase. However, the armature phase is connected to the source only in the zone of polarizing which creates a positive electromagnetic moment. After that, the phase is in the disconnected state without generating electromagnetic torque. To maintain the required torque, it is necessary to increase the linear load on the connected phases, which leads to increased losses and reduced efficiency. Due to the worst energy performance, Single-half-period switching is also excluded from further analysis.

Types of two-half-period switching are distinguished by the time the phase is connected in the inter-switching interval. A distinction should be made between 180-degree switching and 180-(180/m) degree switching.

In the future, we will consider 180-degree switching and 180-(180/m)-degree switching.

At present, there is a steady trend towards an increase in the number of phases of the anchor winding. This is due to the following factors:

- improved energy performance, in particular efficiency;
- indicators that characterize the quality of output parameters are improved, in particular, the pulsation of the electromagnetic moment is reduced;
- increased reliability in case of failures of one or more phases.

Increased reliability is a determining factor when the number of phases increases.

According to the method of connecting multiphase windings to each other, three options are possible: in the “star”, in the “ring”, with independent connection (galvanically isolated phases).

If the number of phases is more than three, when connected to a “star”, the current flows only through the phases that have the highest and lowest potential on the switched keys. This reduces the power of the multiphase BMAMF.

The connection of the winding to the ring is rarely used due to the increased current through the keys. When connecting in a “star” and “ring”, it is difficult to ensure high reliability in case of phase failures.

Galvanically isolated phases require a large number of power keys (four keys per phase), but they provide the greatest reliability in case of open and short circuit

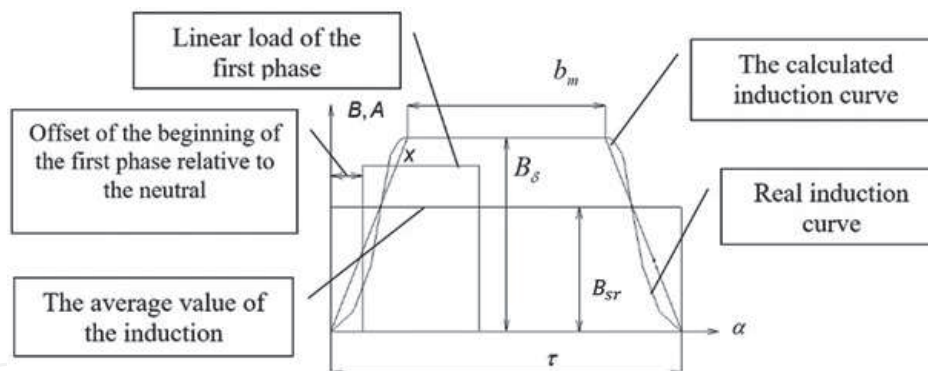


Figure 2.
Representation of air gap induction and linear load.

failures. Taking into account the development trends of power electronics for the production of hybrid assemblies, we choose to focus on the study of this type of connection of multiphase BMAMF windings.

Thus, two-half-period (180-(180/m)-degree switching and two-half-period 180-degree switching with galvanically isolated phases are selected for further analysis.

For the selected switching types, we will carry out the further analysis.

2.1 Analysis of 180-(180/m) - degree commutation for BMAMF with any phases

To analyze the commutation, we determine the interaction of amperes-turns with the magnetic field of permanent magnets at different positions of the armature and inductor relative to each other. In this case, a trapezoidal one with an equivalent amplitude replaces the actual distribution of induction in the air gap [13].

By the pole overlap coefficient, we mean the ratio:

$$\alpha = \frac{b_m}{\tau}, \quad (1)$$

where b_m - width of the pole;

τ - distance between of the neutrals.

The linear load of the phase conductors is represented as rectangles, equal in width to the phase zone, and equal in amplitude to the average linear load of the phase (**Figure. 2**). The analysis is carried out for relative values, taking the base value of the induction amplitude and the average linear load on the average diameter of the axial machine. This representation of an electric machine for analysis should be recognized as traditional.

Figure 3 shows a diagram of the positions of the amperes of the turns in the inter-switching interval for the two pole divisions and the moments of connection and disconnection of the corresponding phases.

We derive the equation of the electromagnetic moment for a generalized axial machine, which is a disk with a distributed current layer that is permeated by a magnetic flux (**Figure 4**).

The equation of an elementary electromagnetic force acting on an infinitesimal section of a generalized axial machine can be written in the following form based on Ampere's law.

$$dF = Bdidr \quad (2)$$

where B – elementary section induction;

di – elementary section current;
 dr – length of an elementary section.

For an elementary moment, we can write the equation

$$dM = rdF = Brdidr, \quad (3)$$

where r – radius of the elementary section location.

Imagine the induction as the product of a base value equal to the amplitude of the induction in the air gap and the relative function of the change in the induction within the pole division.

$$B = B_{\delta}B(\alpha_{el}), \quad (4)$$

where α_{el} – angular coordinate in electrical degrees.

By analogy with induction, we express the linear load function on the average radius of the disk of a generalized axial machine depending on the pole division

$$A(x) = A_{sr}A_i(\alpha_{el}, x), \quad (5)$$

where A_{sr} – the amplitude of the linear load on the average radius of the disk.

$A_i(\alpha_{el}, x)$ – relative function of the linear load change for the i -th phase within the pole division in electrical degrees;

x – offset of the beginning of the first phase relative to the neutral.

Given that there is a relationship between geometric and electrical degrees

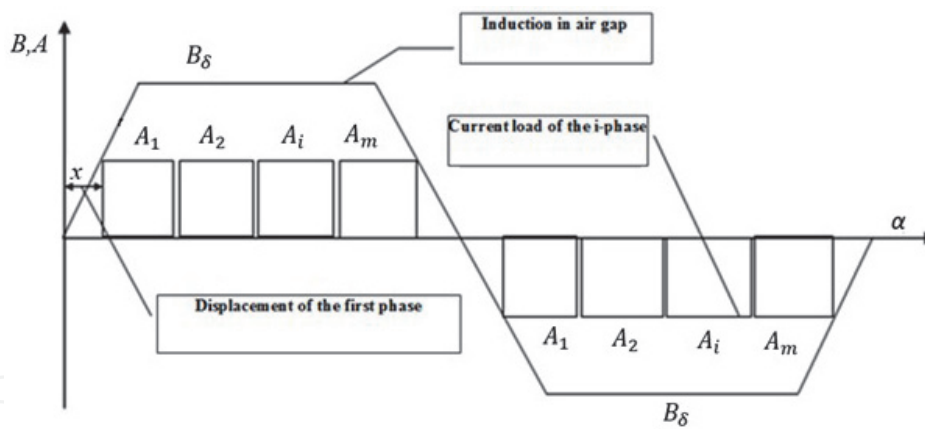


Figure 3.
 The diagram for the $(180-180/m)$ -degree commutation.

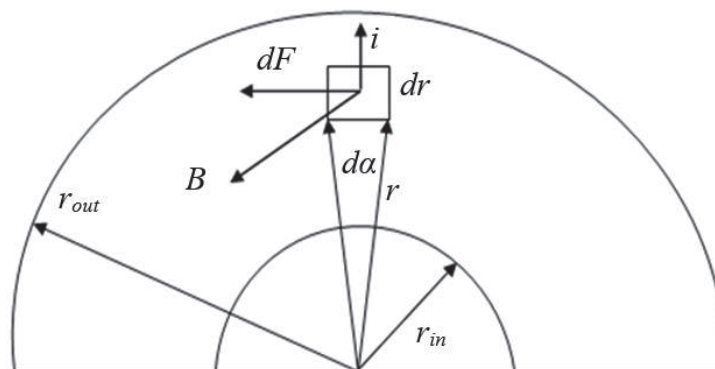


Figure 4.
 Model for axial gap machine.

$$\alpha = 2p\alpha_{el}, \quad (6)$$

where $2p$ – the number of poles of a generalized axial machine.

The expression for the current of an elementary section can be written as follows

$$di(x) = \frac{2\pi r_{sr} A_{sr} A_i(\alpha_{el}, x)}{2\pi r} r 2p d\alpha_{el} = 2p r_{sr} A_{sr} A_i(\alpha_{el}, x) d\alpha_{el}, \quad (7)$$

Substituting (Eq.4) and (Eq.4) in (Eq.3), we obtain an expression for the electromagnetic moment of the elementary section that creates the i -th phase

$$dM_{fi}(x) = 2p r_{sr} A_{sr} B_{\delta} B(\alpha_{el}) A_i(\alpha_{el}, x) r dr d\alpha_{el}. \quad (8)$$

To determine the moment of the i -th phase, we take the integral over the disk surface of a generalized axial machine

$$\begin{aligned} M_{fi}(x) &= \int_{r_{in}}^{r_{out}} \int_0^{2\pi} dM_{fi}(x) = 2p r_{sr} A_{sr} B_{\delta} \int_{r_{in}}^{r_{out}} \int_0^{2\pi} B(\alpha_{el}) A_i(\alpha_{el}) r dr d\alpha_{el} \\ &= \frac{p}{2} A_{sr} B_{\delta} D_{sr}^2 L_{ring} \int_0^{\pi_{el}} B(\alpha_{el}) A_i(\alpha_{el}) d\alpha_{el}, \end{aligned} \quad (9)$$

where D_{sr} – average ring diameter of a generalized axial machine, L_{ring} – ring thickness of the generalized axial machine (**Figure 4**).

For the basic moment value, we take the expression

$$M_b = \frac{p}{2} A_{sr} B_{\delta} D_{sr}^2 L_{ring}. \quad (10)$$

Then the dependence of the relative moment on the displacement of the armature relative to the inductor for the i -th phase will have the form.

$$M_{fi}^* = \int_0^{\pi_{el}} B(\alpha_{el}) A_i(\alpha_{el}, x) d\alpha_{el} \quad (11)$$

Decompose the function of induction and linear load into a harmonic series. We take into account the symmetry of the curves relative to the coordinate axes.

Relative value of induction in the air gap

$$B(\alpha_{el}) = \sum_{n=1}^k a_n \sin(n\alpha_{el}); \quad (12)$$

$$a_n = \frac{2}{\pi_{el}} \left(\int_0^{\frac{\pi_{el}(1-\alpha)}{2}} \frac{2\alpha}{\pi_{el}(1-\alpha)} \sin(n\alpha_{el}) d\alpha_{el} + \int_{\frac{\pi_{el}(1-\alpha)}{2}}^{\frac{\pi_{el}(1-\alpha)}{2} + \pi\alpha} \sin(n\alpha_{el}) d\alpha_{el} + \int_0^{\frac{\pi_{el}(1-\alpha)}{2} + \pi\alpha} \frac{2(1-\alpha)}{\pi_{el}(1-\alpha)} \sin(n\alpha_{el}) d\alpha_{el} \right), \quad (13)$$

where k – number of terms in the harmonic series.

Relative value of the linear load of the i -th phase:

$$A_i(\alpha_{el}, x) = \sum_{n1}^{k1} a_{1n1}(i, x) \sin(n1\alpha_{el}) + b_{1n1}(i, x) \cos(n1\alpha_{el}); \quad (14)$$

$$a_{1n1}(i, x) = \frac{1}{\pi_{el}} \left(\int_{-\pi_{el} + (i-1)\frac{\pi_{el}}{m} + x}^{-\pi_{el} + i\frac{\pi_{el}}{m} + x} (-1) \sin(n1\alpha_{el}) d\alpha_{el} + \int_{(i-1)\frac{\pi_{el}}{m} + x}^{i\frac{\pi_{el}}{m} + x} \sin(n1\alpha_{el}) d\alpha_{el} \right); \quad (15)$$

$$b_{1n1}(i, x) = \frac{1}{\pi_{el}} \left(\int_{-\pi_{el} + (i-1)\frac{\pi_{el}}{m} + x}^{-\pi_{el} + i\frac{\pi_{el}}{m} + x} (-1) \cos(n1\alpha_{el}) d\alpha_{el} + \int_{(i-1)\frac{\pi_{el}}{m} + x}^{i\frac{\pi_{el}}{m} + x} \cos(n1\alpha_{el}) d\alpha_{el} \right), \quad (16)$$

where k_1 – number of terms in the harmonic series;
 i – the number of the phase; m – number of phases.

The total torque of the anchor winding will be created as a sum of the phases torques (one phase is switched of)

$$M_{180-\frac{180}{m}}^*(x) = \sum_{i=1}^{m-1} M_{fi}^*(x). \quad (17)$$

The medium torque for this type of commutation may be described by the following formula

$$M_{sr(180-180/m)}^* = \frac{\int_0^{\frac{\pi_{el}}{m}} M_{180-180/m}^*(x) dx}{\frac{\pi_{el}}{m}}. \quad (18)$$

It is possible to see from diagram 3 that different wires conductors create different torque because they take place in different magnet field conditions. The factor below can estimate the efficiency of anchor wire:

$$K_{ef(180-\frac{180}{m})}(\alpha, m) = \frac{M_{sr(180-180/m)}^*}{\pi_{el}}. \quad (19)$$

Let us name this factor as the efficiency factor of the anchor for $(180-180/m)$ -degree commutation, This factor depends from pole factor and number of the phases. The curves for $(180-180/m)$ -degree commutation (Eq. 19)) are presented in **Figure 5**. The curves analysis shows that it is necessary to increase pole factor and number of the phases for increasing the electromagnetic torque.

The absolute moment may be defined by the following formula

$$M_{sr(180-180/m)} = \frac{\pi}{2} A_{sr} B_{\delta} D_{sr}^2 L_{ring} K_{ef(180-\frac{180}{m})}. \quad (20)$$

The curves analysis shows that it is necessary to increase pole factor and number of the phases for increasing the electromagnetic torque.

2.2 Analysis of 180-degree commutation for BMAMF with any phases

We will use the same harmonic analysis method for 180-degree commutation.

The diagram of the 180-degree commutation is presented in **Figure 6**.

We may use the same formulas (Eq. (9), Eq. (12), Eq. (14)) for induction in the air gap, current load, and torque for the one phase.

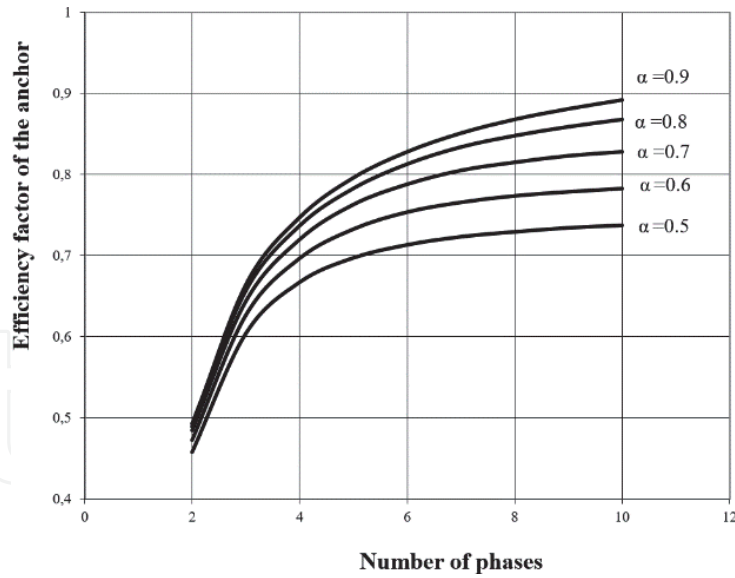


Figure 5.
The dependences of the efficiency factor of the anchor wire for $(180-180/m)$ -degree commutation from pole factor and number of phases.

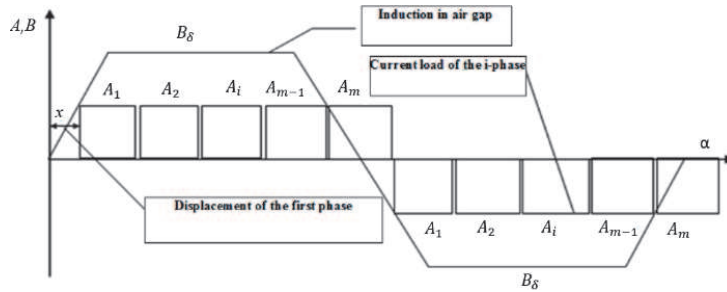


Figure 6.
The diagram for the 180-degree commutation.

For the total relative torque, we may write the following formula (all phases are switched on).

$$M_{180}^*(x) = \sum_{i=1}^m M_{fi}^*(x). \quad (21)$$

The medium torque

$$M_{sr180}^* = \frac{\int_{-\frac{\pi_{el}}{2m}}^{\frac{\pi_{el}}{2m}} M_{180}^*(x) dx}{\frac{\pi_{el}}{m}}. \quad (22)$$

The efficiency factor of the anchor for 180-degree commutation

$$K_{ef180}(\alpha, m) = \frac{M_{sr180}^*}{\pi_{el}}. \quad (23)$$

The curves for this factor (Eq.(23)) are presented in the **Figure 7**.
The absolute moment may be defined by the following formula

$$M_{sr180} = \frac{\pi}{2} A_{sr} B_{\delta} D_{sr}^2 L_{ring} K_{ef180}. \quad (24)$$

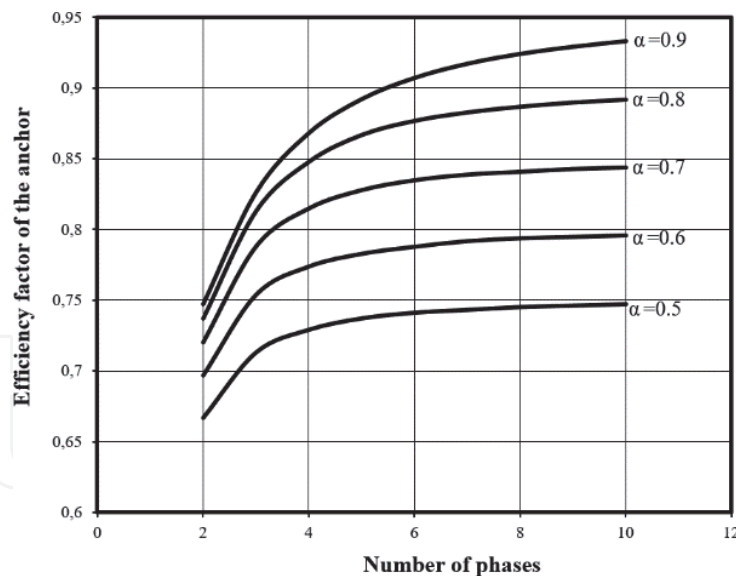


Figure 7.
 The dependences of the efficiency factor of the anchor for 180-degree commutation from pole factor and number of phases.

We can create the same conclusion for this type of the commutation. It is necessary to increase the pole factor and number of the phases for increasing the electromagnetic torque.

Let us compare the efficiency of this type commutation. The electromagnetic torque will be the criteria for this analysis.

2.3 The compare of the (180–180/m)-degree commutation and 180- degree commutation for BMAMF with any phases

We will use the same sizes and the same current load for both types of commutation.

The ratio of the total electromagnetic torques is

$$\frac{M_{sr180}}{M_{sr(180-180/m)}} = \frac{K_{ef180}}{K_{ef(180-\frac{180}{m})}} \quad (25)$$

Let us compare both commutations for pole factor 0.8. It is typical pole factor for brushless machine. The curve of this analysis is shown in the **Figure 8**.

The curve shows that 180-degree commutation has the advantage but for big numbers of phases this advantage is decreasing. It is possible to do this compare for another type of the pole factors and we will have the same conclusion.

We show the advantage of the 180-degree commutation with using the electromagnetic torque.

The studies have shown that to increase the efficiency of the system it is necessary to increase the number of phases and use the 180-degree commutation but it is necessary to say that the cost of electronic control system will be increasing with increasing the number of phases. Therefore, the researcher has to take a mind this information when he will create the real equipment.

It should be noted that as the number of phases increase, the difference in efficiency of these type of commutation decreases too. Since the (180–180/m)-degree commutation is simpler to implement, so it can be chosen for practice.

The study can define the following results:

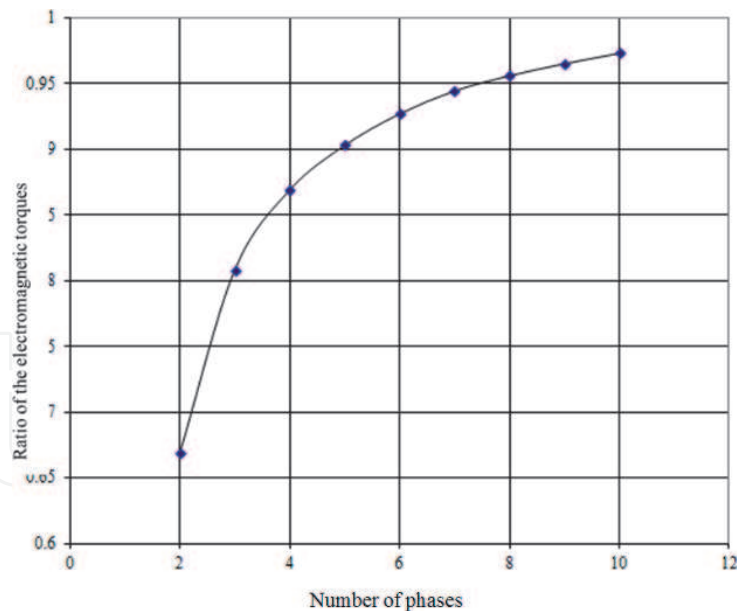


Figure 8.

The compare of the $(180-180/m)$ -degree commutation with the 180 -degree commutation for pole factor 0.8 .

1. The electromagnetic torque will be increasing for both type commutations with increasing the number of phases.
2. 180 -degree commutation has the advantage with different phases and different pole factors if compare it with the $(180-180/m)$ -degree commutation.

These conclusions determine the trend of increasing efficiency, but in practice, it is necessary to calculate the price for choosing the best type of commutation.

3. Analysis of electromagnetic power of various designs of the BMAMF

BMAMF have a large number of designs. Different designs in the same dimensions develop different torque and power. To compare the effectiveness of various designs, we will classify them.

3.1 Classification of various BMAMF designs

The shape of active elements that create an electromagnetic moment can classify a large number of design modifications of BMAMF. The shape of permanent magnets may be cylindrical, prismatic and segmental magnets. BMAMF phase coils can have ring, trapezoidal, wave, and toroid shapes. The combination of various permanent magnet shapes with armature winding shapes creates a variety of BMAMF designs [14, 15]. The classification of BMAMF structures is shown in **Figure 9**.

The main design versions of BMAMF active parts with various forms of magnets and coils are shown below. On their basis, it is possible to build various design modifications. Let us call these models basic. **Figure 10** shows a BMAMF with cylindrical magnets and ring coils. **Figure 11** shows a BMAMF with segment magnets and trapezoidal coils. **Figure 12** shows a BMAMF with segment magnets and toroid coils.

The development of computational models for the above structures has its own peculiarities. Let us output the values of the electromagnetic moment and electromagnetic power for the basic versions shown in **Figure 10–13**.

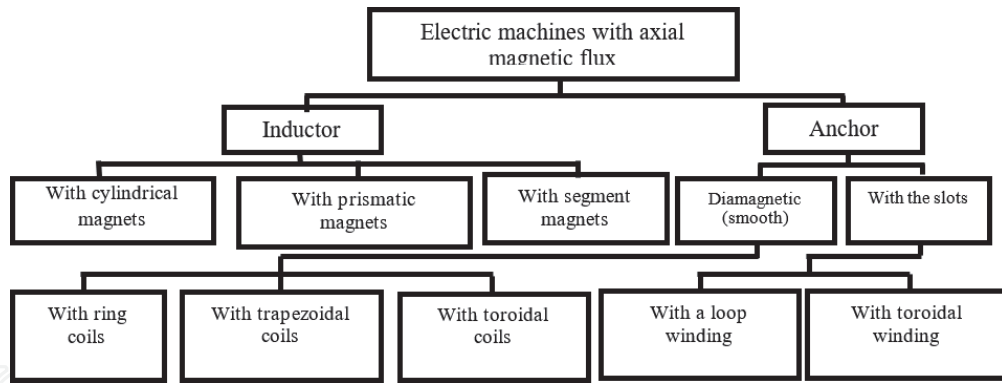


Figure 9.
Classification of BMAMF.

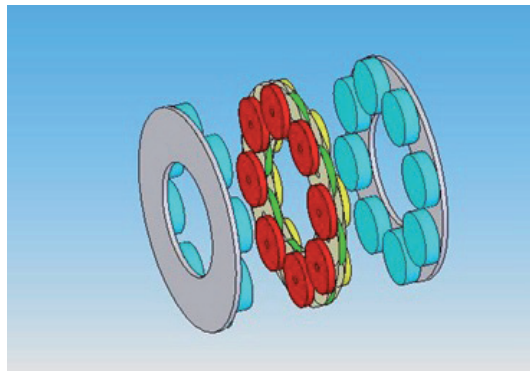


Figure 10.
BMAMF with cylindrical magnets and a smooth anchor with ring coils.

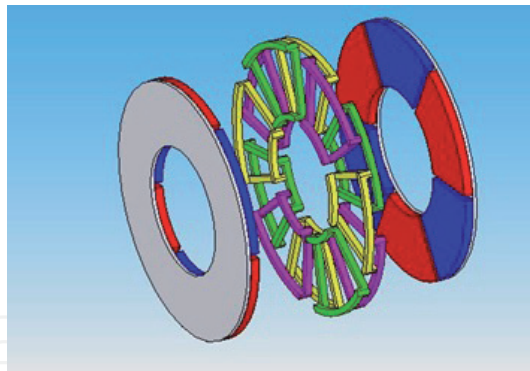


Figure 11.
BMAMF with segment magnets and a smooth anchor with trapezoidal.

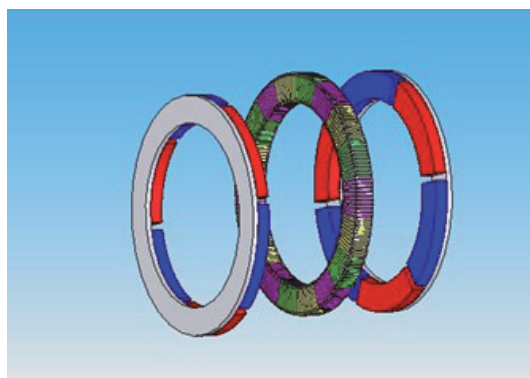


Figure 12.
BMAMF with segment magnets and a smooth armature with toroidal coils.

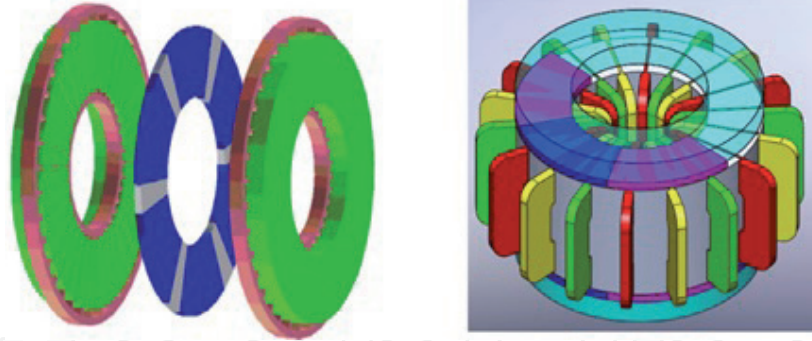


Figure 13.
BMAMF with segment magnets and toothed anchor.

3.2 Electromagnetic torque and electromagnetic power for BMAMF with cylindrical magnets and smooth armature with ring coils

Let us define the electromagnetic moment of the phase in the position at which it has the maximum value. This is the position at which the axis of the ring coil coincides with the geometric neutral. A sketch of the magnetic system and the armature winding is shown in **Figure 14**. To facilitate reference to the dependencies given below, we denote this design as model 1.

The real value of the magnetic induction in the gap is replaced by its average value, assuming that it does not change within the pole division.

The ratio between the maximum induction and the average induction is determined by the formula

$$B_{sr} = B_{\delta} \frac{S_{pole}}{S_{\tau}}, \quad (26)$$

where S_{pole} – surface of the pole,
 S_{τ} – area of the pole division/.

Let us choose an arbitrary j turn with an anchor current i_a . On this turn, we select an elementary conductor with length dl on the left and right sides. These elementary conductors will be affected by elementary forces, like conductors in a magnetic field, which will be directed to the center of the anchor coil. These forces can be decomposed into components on the X-axis and on the y-axis. The forces on the Y-axis will compensate for each other as equal in magnitude and opposite in direction.

The electromagnetic moment will only be created by forces directed along the x-axis. Elementary moment of the j -th turn:

$$dM_j = dM_{\alpha 1j} + dM_{\alpha 2j}, \quad (27)$$

where

$$dM_{\alpha 1j} = dF_{\alpha 1xj} (R_{sr} + r_{vj} \sin \alpha_1) = i_a B_{sr} r_{vj} \cos \alpha_1 (R_{sr} + r_{vj} \sin \alpha_1) d\alpha_1. \quad (28)$$

$$dM_{\alpha 2j} = dF_{\alpha 2xj} (R_{sr} + r_{vj} \sin \alpha_1) = i_a B_{sr} r_{vj} \cos \alpha_2 (R_{sr} + r_{vj} \sin \alpha_2) d\alpha_2. \quad (29)$$

where $dF_{\alpha 1xj}, dF_{\alpha 2xj}$ – elementary forces acting on the left and right halves of the coil;

$$\begin{aligned}
 M_{max \ mod1(180-\frac{180}{m})} &= M_{fmod1} \sum_{i=1}^{m-1} \cos \left(-\frac{\pi}{2} + \frac{\pi}{m} + \frac{\pi}{m}(i-1) \right) \\
 &= \frac{1}{2} i_a B_{sr} D_{sr} L_{ring} p W_s \sum_{i=1}^{m-1} \cos \left(-\frac{\pi}{2} + \frac{\pi}{m} + \frac{\pi}{m}(i-1) \right) \\
 &= \frac{\pi}{2} A_{sr} B_{sr} D_{sr}^2 L_{ring} K_{mod1(180-\frac{180}{m})}, \tag{33}
 \end{aligned}$$

where $K_{mod1(180-\frac{180}{m})}$ – the coefficient of efficiency of model 1 for $(180-180/m)$ -degree commutation

$$K_{mod1(180-\frac{180}{m})} = \frac{\sum_{i=1}^{m-1} \cos \left(-\frac{\pi}{2} + \frac{\pi}{m} + \frac{\pi}{m}(i-1) \right)}{2m}. \tag{34}$$

The graphical dependence of this coefficient on the number of phases for $(180-180/m)$ - degree commutation (Eq. (34)) is shown in **Figure 15**.

For 180-degree commutation

$$\begin{aligned}
 M_{max \ mod1(180)} &= M_{fmod1} \sum_{i=1}^m \cos \left(-\frac{\pi}{2} + \frac{\pi}{2m} + \frac{\pi}{m}(i-1) \right) \\
 &= \frac{1}{2} i_a B_{sr} D_{sr} L_{ring} p W_s \sum_{i=1}^m \cos \left(-\frac{\pi}{2} + \frac{\pi}{2m} + \frac{\pi}{m}(i-1) \right) \\
 &= \frac{\pi}{2} A_{sr} B_{sr} D_{sr}^2 L_{ring} K_{mod1(180)}. \tag{35}
 \end{aligned}$$

where $K_{mod1(180)}$ – efficiency coefficient of model 1 on the number of phases for 180- degree commutation

$$K_{mod1(180)} = \frac{\sum_{i=1}^m \cos \left(-\frac{\pi}{2} + \frac{\pi}{2m} + \frac{\pi}{m}(i-1) \right)}{2m}. \tag{36}$$

The graphical dependence of this coefficient on the number of phases for 180-degree switching (Eq.(36)) is shown in **Figure 16**.

Physical meaning of the efficiency coefficients of the model is to determine the share that the phases invest in creating the maximum moment.

Let us determine the average electromagnetic moment and electromagnetic power for the model1 BMAMF for various switching options, taking into account the efficiency coefficients derived above.

For $(180-180/m)$ - degree commutation:

$$M_{sr \ mod1(180-\frac{180}{m})} = \frac{\pi}{2} A_{sr} B_{sr} D_{sr}^2 L_{ring} K_{mod1(180-\frac{180}{m})} K_{ef(180-\frac{180}{m})}; \tag{37}$$

$$P_{el \ mod1(180-\frac{180}{m})} = \frac{\pi}{2} A_{sr} B_{sr} \omega D_{sr}^2 L_{ring} K_{mod1(180-\frac{180}{m})} K_{ef(180-\frac{180}{m})}, \tag{38}$$

where ω – rotation speed in rad/s.

For 180 - degree commutation:

$$M_{sr \ mod1(180)} = \frac{\pi}{2} A_{sr} B_{sr} D_{sr}^2 L_{ring} K_{mod1(180)} K_{ef180}; \tag{39}$$

$$P_{el \ mod1(180)} = \frac{\pi}{2} A_{sr} B_{sr} \omega D_{sr}^2 L_{ring} K_{mod1(180)} K_{ef180}. \tag{40}$$

It is of theoretical interest to choose the most efficient type of switching for model 1 with the same electromagnetic loads and in the same dimensions. For

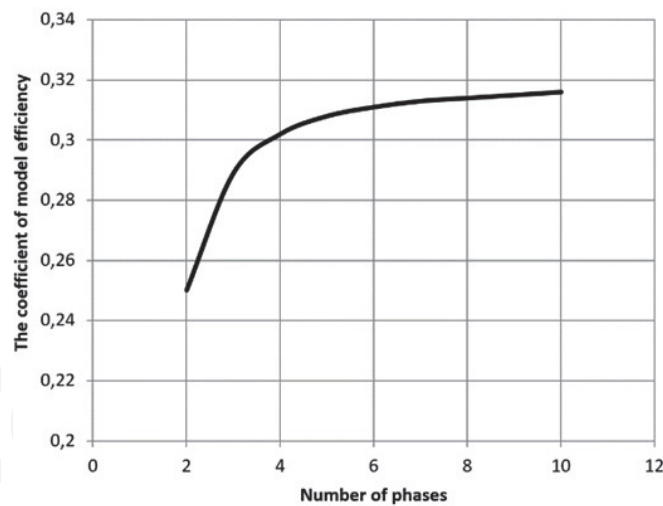


Figure 15.
 Dependence of the efficiency coefficient of model 1 on the number of phases for $(180-180/m)$ - degree commutation.

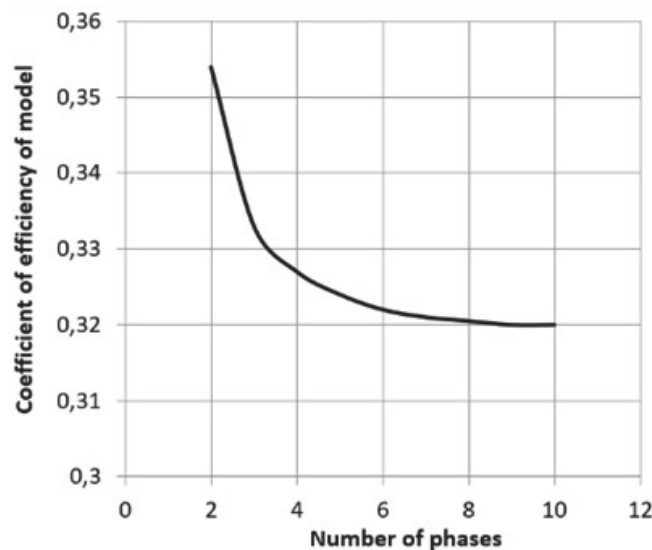


Figure 16.
 Dependence of the efficiency coefficient of model 1 on the number of phases for 180 - degree commutation.

quantitative evaluation, we introduce the commutation comparison coefficient as the ratio of electromagnetic powers $(180-180/m)$ - degree commutation and 180-degree commutation:

$$K_{comp_com_mod1} = \frac{P_{el\ mod1(180-\frac{180}{m})}}{P_{el\ mod1(180)}} = \frac{K_{mod1(180-\frac{180}{m})}K_{ef(180-\frac{180}{m})}}{K_{mod1(180)}K_{ef180}} \quad (41)$$

The graphical dependence of this coefficient on the number of phases is shown in **Figure 17**.

The dependence analysis shows that for model 1, 180-degree commutation has an advantage with a small number of phases. As the number of phases increases, this advantage decreases.

3.3 Electromagnetic moment and electromagnetic power for BMAMF with segment magnets and trapezoidal coils

A sketch of the magnetic system and the BAMF armature winding of this design is shown in **Figure 18**. Let us refer to this design as model 2.

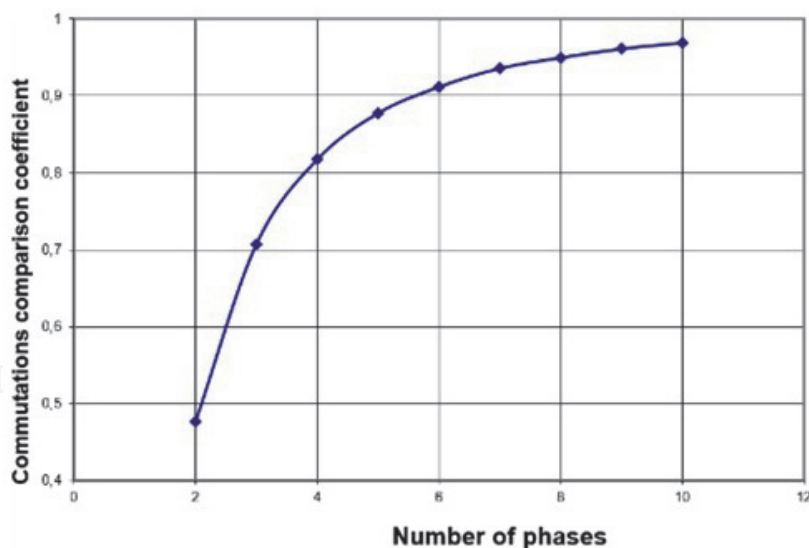


Figure 17.
Dependence of the commutations comparison coefficient for model 1.

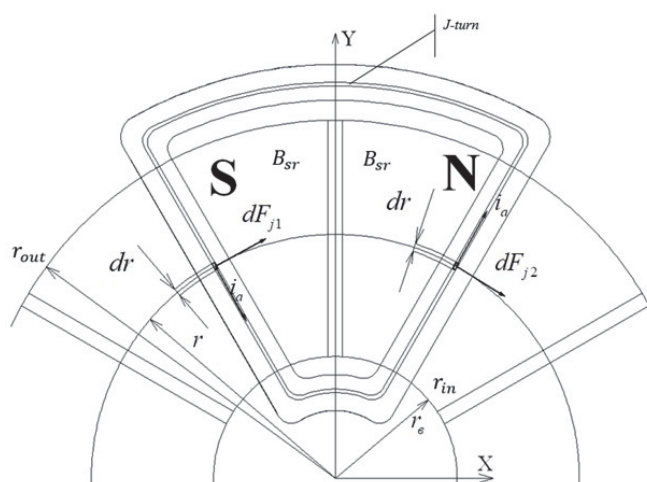


Figure 18.
Sketch of the magnetic system and armature winding BMAMF with segment magnets and trapezoidal armature windings.

Let us select elementary conductors of length dr on an arbitrary j -turn of the winding and define elementary moments for them. They will be a function of the angular position and radius of the elementary section.

$$dM(\alpha, r)_{1j} = dM(\alpha, r)_{2j} = i_a B(\alpha) r dr, \quad (42)$$

where r – radius, where the elementary conductor is located.
Electromagnetic moment j -th of the turn

$$M(\alpha, r)_j = \int_{r_{in}}^{r_{out}} dM(\alpha, r)_{1j} + \int_{r_{in}}^{r_{out}} dM(\alpha, r)_{2j} = 2i_a B(\alpha) \frac{r_{out}^2 - r_{in}^2}{2}. \quad (43)$$

Electromagnetic moment of the phase section

$$M(\alpha, r)_{W_S} = \sum_{j=1}^{W_S} dM(\alpha, r)_j = 2i_a B(\alpha) \frac{r_{out}^2 - r_{in}^2}{2} W_S. \quad (44)$$

Electromagnetic moment of an arbitrary i -th phase

$$M(\alpha, r)_{fi\ mod2} = M(\alpha, r)_{Wsp} = 2i_a B(\alpha) \frac{r_{out}^2 - r_{in}^2}{2} W_{sp}. \quad (45)$$

The maximum moment of all phases in the intercommutation interval will depend on the pole overlap coefficient of the magnetic system, determined by equation (Eq. (1)), the number of phases, and the type of switching. Let us determine the influence of these factors on model 2. By analogy with model 1, we introduce the efficiency coefficient of model 2, which is the ratio of the maximum moment of the armature winding at the real pole overlap coefficient to the maximum moment at the theoretical pole overlap coefficient equal to 1.0. As a rule, the distance between the side faces of permanent magnets is the same on the inner and outer diameters. In this case, the pole overlap coefficient changes linearly when moving from the inner diameter to the outer one. Therefore, analytical expressions can be derived for the average diameter of a ring with magnets and further use this linear relationship.

For $(180-180/m)$ -degree commutation, the efficiency coefficient of the model is defined by the following expression

$$K_{mod2(180-\frac{180}{m})}(\alpha, m) = \frac{M(\alpha_{sr}, m)_{(180-\frac{180}{m})\ max}}{M(\alpha_{sr} = 1, m)_{(180-\frac{180}{m})\ max}} = \frac{M(\alpha_{sr}, m)_{(180-\frac{180}{m})\ max}^*}{\frac{\pi}{m}(m-1)}, \quad (46)$$

where α_{sr} – real coefficient of pole overlap on the average ring diameter of the magnetic system;

$M(\alpha_{sr}, m)_{(180-\frac{180}{m})\ max}$ – maximum moment of the armature winding at the real coefficient of pole overlap;

$M(\alpha_{sr} = 1, m)_{(180-\frac{180}{m})\ max}$ – the maximum moment of the armature winding with a pole overlap coefficient equal to 1, which is only theoretically possible;

$M(\alpha_{sr}, m)_{(180-\frac{180}{m})\ max}^*$ – relative value of the maximum moment of the armature winding at the real coefficient of pole overlap.

The relative value of the maximum moment of the armature winding can be determined from the expression (Eq. (17)) for the offset of the armature from the neutral by $x = \frac{\pi}{2m}$ (see **Figure 19**)

$$M(\alpha_{sr}, m)_{(180-\frac{180}{m})\ max}^* = M_{(180-\frac{180}{m})}^* \left(\frac{\pi}{2m} \right) = \sum_{i=1}^{m-1} M_{fi}^* \left(\frac{\pi}{2m} \right). \quad (47)$$

The physical meaning of the efficiency coefficient of model 2 is similar to the coefficient for model 1. The graphical dependence of the coefficient for $(180-180/m)$ - degree switching (Eq.(46)) is shown in **Figure 20**.

Taking into account the introduced efficiency coefficient of the model, we can write the following expression of the maximum electromagnetic moment for $(180-180/m)$ - degree commutation

$$\begin{aligned} M_{\max\ mod2(180-\frac{180}{m})} &= \sum_{i=1}^{m-1} M(\alpha, m)_{fi\ mod2} K_{mod2(180-\frac{180}{m})} \\ &= 2i_a B_\delta \frac{r_{out}^2 - r_{in}^2}{2} W_{sp} K_{mod2(180-\frac{180}{m})} = \frac{\pi}{2} A_{sr} B_\delta D_{sr}^2 L_{ring} K_{mod2(180-\frac{180}{m})}. \end{aligned} \quad (48)$$

Average electromagnetic moment and electromagnetic power for $(180-180/m)$ - degree commutation

$$\begin{aligned} M_{srmod2(180-\frac{180}{m})} &= M_{\max mod2(180-\frac{180}{m})} K_{ef(180-\frac{180}{m})} \\ &= \frac{\pi}{2} A_{sr} B_{\delta} D_{sr}^2 L_{ring} K_{mod2(180-\frac{180}{m})} K_{ef(180-\frac{180}{m})}; \end{aligned} \quad (49)$$

$$P_{elmod2(180-\frac{180}{m})} = \frac{\pi}{2} A_{sr} B_{\delta} \omega D_{sr}^2 L_{ring} K_{mod2(180-\frac{180}{m})} K_{ef(180-\frac{180}{m})}. \quad (50)$$

By analogy, we derive the equations for 180-degree commutation.

For 180-degree switching, the efficiency coefficient of the model is defined by the following expression

$$K_{mod2(180)}(\alpha, m) = \frac{M(\alpha_{sr}, m)_{(180)max}}{M(\alpha_{sr} = 1, m)_{(180)max}} = \frac{M(\alpha_{sr}, m)_{(180)max}^*}{\pi}, \quad (51)$$

where $M(\alpha_{sr}, m)_{(180)max}$ – maximum moment of the armature winding at the real coefficient of pole overlap;

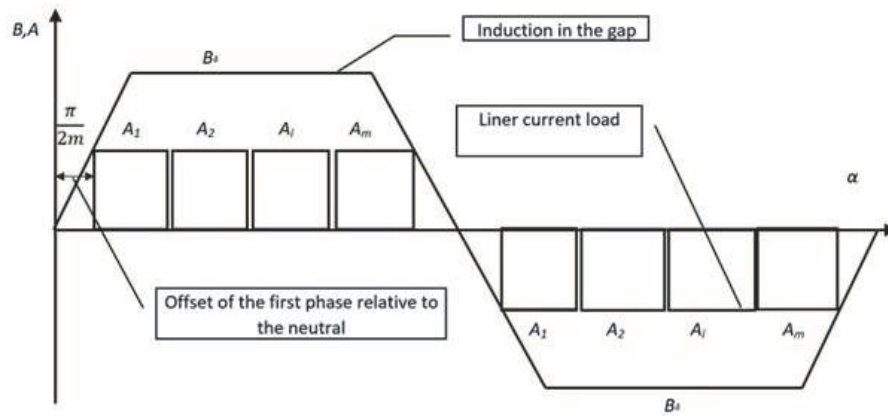


Figure 19. Position of multiphase armature winding sections at the maximum electromagnetic moment for $(180-180/m)$ -degree commutation.

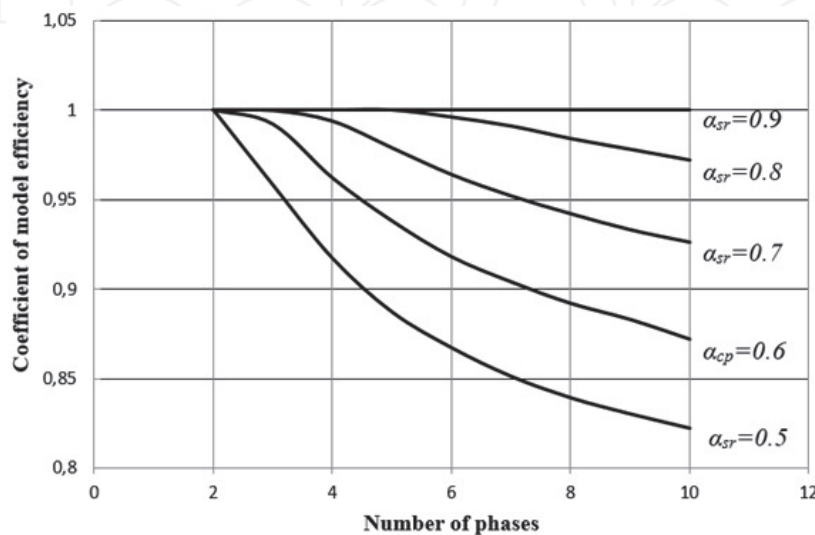


Figure 20. Efficiency coefficient of model 2 for $(180-180/m)$ - degree switching at different values of the number of phases and the coefficient of pole overlap on the average diameter of the ring of the magnetic system.

$M(\alpha_{sr} = 1, m)_{(180)max}$ – maximum moment of the armature winding with a pole overlap coefficient equal to 1, which is only theoretically possible;

$M(\alpha_{sr}, m)_{(180)max}^*$ – relative value of the maximum moment of the armature winding at the real coefficient of pole overlap.

Efficiency coefficient of model 2 for 180 - degree switching at different the coefficient of pole overlap on the average diameter of the ring of the magnetic system (Eq. (51)) is shown at **Figure 22**. We can see that this coefficient does not depend on the number of phases.

The relative value of the maximum moment of the armature winding can be determined from the expression (Eq.(21)) for the zero offset of the armature from the neutral (see **Figure 21**)

$$M(\alpha_{sr}, m)_{(180)max}^* = M_{(180)max}^*(0) = \sum_{i=1}^m M_{fi}^*(0). \quad (52)$$

Maximum electromagnetic torque for 180-degree commutation

$$\begin{aligned} M_{\max mod2(180)} &= \sum_{i=1}^m M(\alpha.r)_{fimax mod2(180)} K_{mod2(180)} = 2i_a B_\delta \frac{r_{out}^2 - r_{in}^2}{2} W_{sp} K_{mod2(180)} \\ &= \frac{\pi}{2} A_{sr} B_\delta D_{sr}^2 L_{ring} K_{mod2(180)}. \end{aligned} \quad (53)$$

The average electromagnetic torque and electromagnetic power for 180-degree commutation

$$M_{srmod2(180)} = M_{\max mod2(180)} K_{ef(180)} = \frac{\pi}{2} A_{sr} B_\delta D_{sr}^2 L_{ring} K_{mod2(180)} K_{ef(180)}; \quad (54)$$

$$P_{elmod2(180)} = \frac{\pi}{2} A_{sr} B_\delta \omega D_{sr}^2 L_{ring} K_{mod2(180)} K_{ef(180)}. \quad (55)$$

By analogy with the previous analysis, for quantitative evaluation, we introduce the switching comparison coefficient, as the ratio of electromagnetic powers (180–180/m) - degree commutation and 180-degree commutation:

$$K_{comp_com_mod2} = \frac{P_{el mod2(180-\frac{180}{m})}}{P_{el mod2(180)}} = \frac{K_{mod2(180-\frac{180}{m})} K_{ef(180-\frac{180}{m})}}{K_{mod2(180)} K_{ef180}}. \quad (56)$$

The graphical dependence of this coefficient on the number of phases and the coefficient of the pole arc (Eq.(56)) is shown in **Figure 23**.

It should be noted that such a comparative analysis makes sense only for the same electromagnetic loads: induction in the air gap and linear load on the average diameter of the disk of the magnetic system.

These dependencies are of great practical importance. Their analysis shows that for the same electromagnetic loads, magnetic systems with a high value of the pole overlap coefficient have an advantage for any number of phases. Graphic dependences of the switching comparison coefficient are below 1.0. However, for magnetic systems with a pole overlap coefficient of 0.7–0.5, which is very typical for practice, the advantage is (180–180/m) - degree commutation for the number of phases starting from 3 and higher.

Given that (180–180/m) - degree commutation has a simpler and cheaper technical implementation, this theoretical conclusion is of great practical importance.

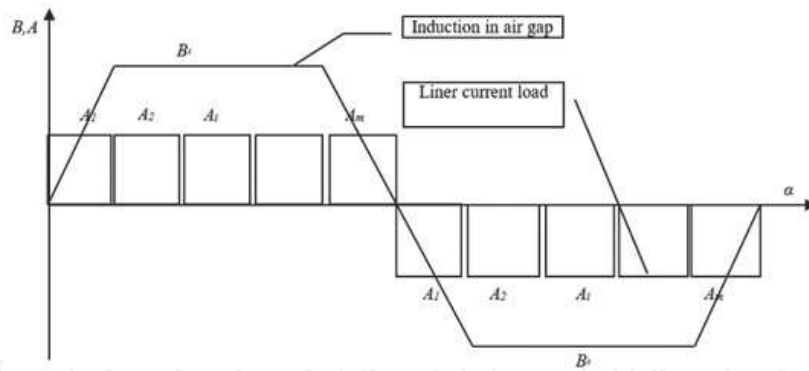


Figure 21. Position of multiphase armature winding sections at the maximum electromagnetic moment for 180-degree commutation.

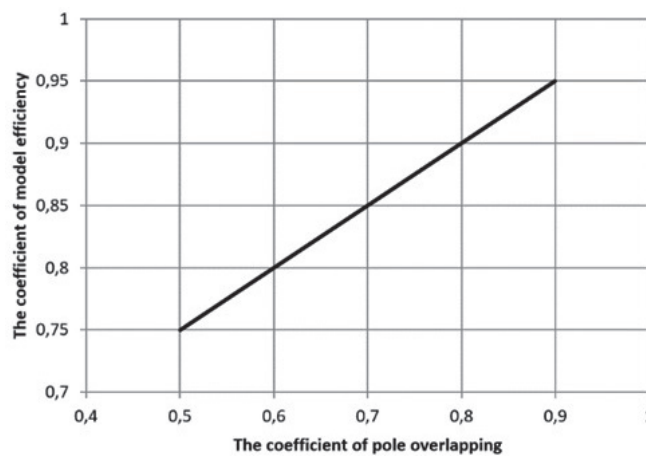


Figure 22. The efficiency coefficient of model 2 for 180-degree commutation at different values of the pole overlap coefficient on the average diameter of the ring of the magnetic system.

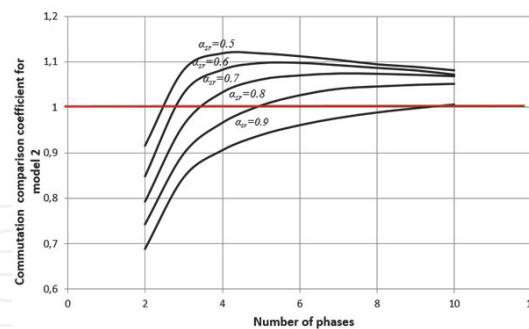


Figure 23. Dependence of the comparison coefficient (180–180/m) - degree commutation and 180-degree commutation for model 2.

3.4 Electromagnetic moment and electromagnetic power for BMAMF with segment magnets and toroidal coils

The analysis will be carried out by analogy with the previous models. A sketch of the magnetic system and armature winding BMAMF of this design is shown in **Figure 24**. Let us designate this design as model 3.

Let us select an elementary conductor of length dr on an arbitrary j -th turn of the winding and determine the elementary moment for it.

$$dM(\alpha, r)_j = i_a B(\alpha) r dr. \quad (57)$$

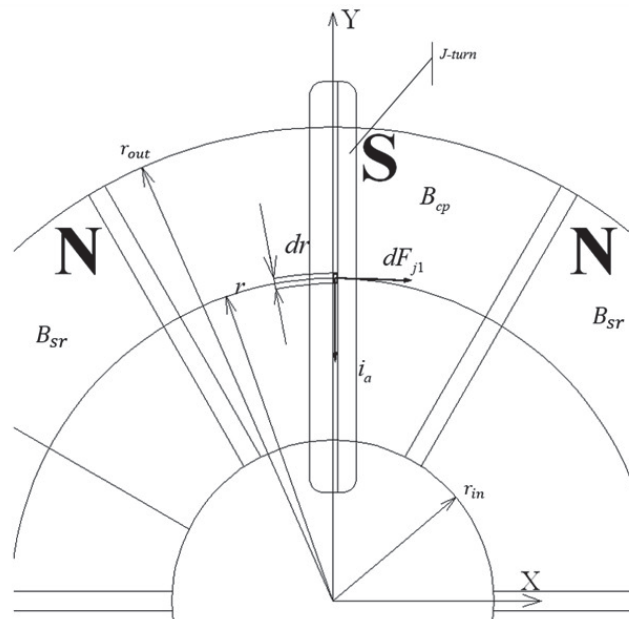


Figure 24. Sketch of the magnetic system and armature windings BMAMF with segment magnets toroidal armature windings.

Electromagnetic moment j -th of the turn

$$M(\alpha, r)_j = \int_{r_{in}}^{r_{out}} dM(\alpha, r)_j = 2i_a B(\alpha) \frac{r_{out}^2 - r_{in}^2}{2}. \quad (58)$$

Electromagnetic moment of the phase section

$$M(\alpha, r)_{W_S} = \sum_{j=1}^{W_S} dM(\alpha, r)_j = 2i_a B(\alpha) \frac{r_{out}^2 - r_{in}^2}{2} W_S. \quad (59)$$

Maximum value of the electromagnetic moment of an arbitrary i -th phase

$$M(\alpha, r)_{f_{mod3}} = M(\alpha, r)_{W_S p} = 2i_a B(\alpha) \frac{r_{out}^2 - r_{in}^2}{2} W_S 2p. \quad (60)$$

By analogy with model 2, we introduce the efficiency coefficient of model 3, which is the ratio of the maximum moment of the armature winding at the real pole overlap coefficient to the maximum moment at the theoretical pole overlap coefficient equal to 1.0. It should be noted that the electromagnetic moment for model 3 is 2 times higher than the electromagnetic moment of model 1. This can be seen from the comparison of equation (Eq. (47)) and equation (Eq. (61)). From a physical point of view, this is because with the same external and internal diameters of the magnetic system, the electromagnetic moment in model 3 is created from 2 sides. We will consider this in the following equations.

For $(180-180/m)$ -degree communication the efficiency coefficient of the model is defined by the following expression

$$K_{mod3(180-\frac{180}{m})}(\alpha, m) = \frac{M(\alpha_{sr}, m)_{(180-\frac{180}{m})max}}{M(\alpha_{sr} = 1, m)_{(180-\frac{180}{m})max}} = \frac{2M(\alpha_{sr}, m)_{(180-\frac{180}{m})max}^*}{\frac{\pi}{m}(m-1)}. \quad (61)$$

The relative value of the maximum moment of the armature winding, which is created on one side of the working air gap, can be determined from the expression (Eq. (17)), for the displacement of the armature from the neutral poles by an amount $x = \frac{\pi}{2m}$.

The graphical dependence of the coefficient for (180–180/m) - degree commutation is shown in **Figure 25**.

Maximum electromagnetic torque for (180–180/m)-degree commutation

$$M_{\max \text{mod}3(180-\frac{180}{m})} = \sum_{i=1}^{m-1} M(\alpha, m)_{fi \text{ mod}3} K_{\text{mod}3(180-\frac{180}{m})} = 2i_a B_\delta \frac{r_{\text{out}}^2 - r_{\text{in}}^2}{2} W_{sp} K_{\text{mod}3(180-\frac{180}{m})} = \frac{\pi}{2} A_{sr} B_\delta D_{sr}^2 L_{ring} K_{\text{mod}3(180-\frac{180}{m})}. \quad (62)$$

Average electromagnetic moment and electromagnetic power for (180–180/m) - degree commutation, based on the above

$$M_{\text{srmod}3(180-\frac{180}{m})} = M_{\max \text{mod}3(180-\frac{180}{m})} K_{ef(180-\frac{180}{m})} = \frac{\pi}{2} A_{sr} B_\delta D_{sr}^2 L_{ring} K_{\text{mod}3(180-\frac{180}{m})} K_{ef(180-\frac{180}{m})} \quad (63)$$

$$P_{\text{elmod}3(180-\frac{180}{m})} = \frac{\pi}{2} A_{sr} B_\delta \omega D_{sr}^2 L_{ring} K_{\text{mod}3(180-\frac{180}{m})} K_{ef(180-\frac{180}{m})}. \quad (64)$$

By analogy, we derive the equations for 180-degree switching.

For 180-degree commutation the efficiency coefficient of the model is defined by the following expression

$$K_{\text{mod}3(180)}(\alpha, m) = \frac{M(\alpha_{sr}, m)_{(180) \max}}{M(\alpha_{sr} = 1, m)_{(180) \max}} = \frac{2M(\alpha_{sr}, m)_{(180) \max}^*}{\pi}. \quad (65)$$

The relative value of the maximum moment of the armature winding can be determined from the expression (1.16) for the zero offset of the armature from the neutral (see **Figure 21**).

By analogy with model 2, the efficiency coefficient of model 3 for this type of switching will not depend on the number of phases and will be determined only by the value of the overlap coefficient on the average ring diameter of the magnetic system. The graphical dependence of this coefficient is shown in **Figure 26**.

Maximum electromagnetic torque for 180-degree commutation

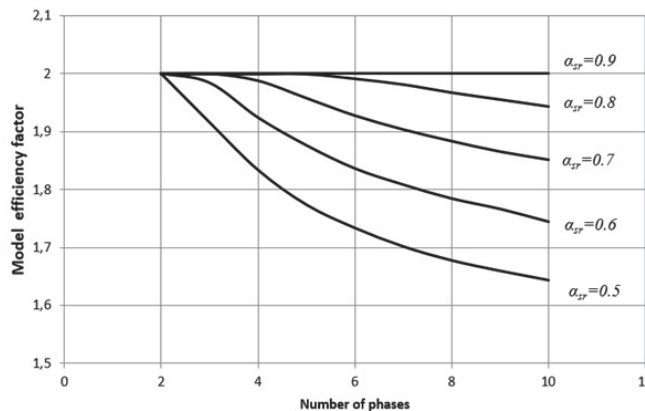


Figure 25.

The efficiency coefficient of model 3 for (180–180/m) - degree commutation at different values of the number of phases and the coefficient of pole overlap on the average diameter of the ring of the magnetic system.

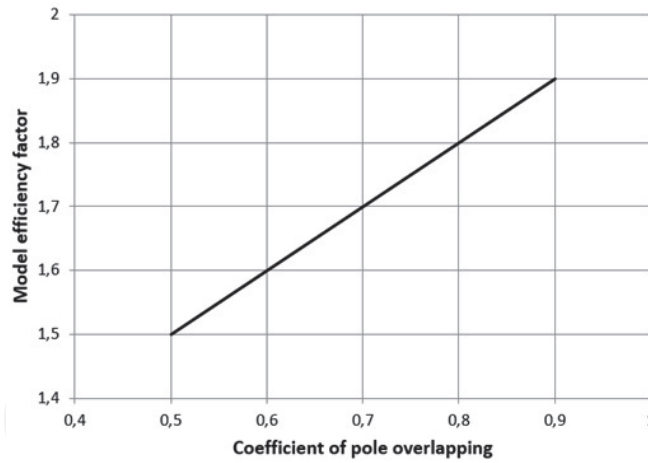


Figure 26.

Model 3 efficiency coefficient for 180-degree commutation with different values of the pole overlap coefficient on the average ring diameter of the magnetic system.

$$\begin{aligned}
 M_{\max \text{mod}3(180)} &= \sum_{i=1}^m M(\alpha.r)_{f_{\max \text{mod}3(180)}} K_{\text{mod}3(180)} = 2i_a B_\delta \frac{r_{\text{out}}^2 - r_{\text{in}}^2}{2} W_{sp} K_{\text{mod}3(180)} \\
 &= \frac{\pi}{2} A_{sr} B_\delta D_{sr}^2 L_{ring} K_{\text{mod}3(180)}.
 \end{aligned}
 \tag{66}$$

The average electromagnetic torque and electromagnetic power for 180-degree commutation

$$M_{\text{srmod}3(180)} = M_{\max \text{mod}3(180)} K_{ef(180)} = \frac{\pi}{2} A_{sr} B_\delta D_{sr}^2 L_{ring} K_{\text{mod}3(180)} K_{ef(180)}; \tag{67}$$

$$P_{\text{elmod}3(180)} = \frac{\pi}{2} A_{sr} B_\delta \omega D_{sr}^2 L_{ring} K_{\text{mod}3(180)} K_{ef(180)}. \tag{68}$$

By analogy with the previous analysis, for quantitative evaluation, we introduce the switching comparison coefficient for model 3 as the ratio of electromagnetic powers (180–180/m) - degree communication and 180-degree commutation:

$$K_{\text{comp_com_mod}3} = \frac{P_{\text{el mod}3(180-\frac{180}{m})}}{P_{\text{el mod}3(180)}} = \frac{K_{\text{mod}3(180-\frac{180}{m})} K_{ef(180-\frac{180}{m})}}{K_{\text{mod}3(180)} K_{ef180}}. \tag{69}$$

Since the analytical dependences of the efficiency coefficient for model 2 and model 3 are multiples of 2, the graphical dependence of this coefficient on the number of phases for different values of the pole overlap coefficient completely coincides with the curves shown in **Figure 23** for model 3, we can draw conclusions similar to those for model 2 regarding the advantages of commutations types when changing the number of phases and the pole overlap coefficient.

3.5 Electromagnetic moment and electromagnetic power for BMAMF with segment magnets and toothed anchor

The armature winding for this design can be made by analogy with a radial design (wave or loop) or toroidal. It should be noted that the windings for these three options would differ only in the shape of the frontal parts, which will only affect the calculation of active and inductive resistances. The active zone with copper (the groove-tooth zone) will be identical for all variants. Consequently, the electromagnetic processes of mutual conversion of electromagnetic and mechanical energy will also be identical. This allows you to combine all design types with a

toothed anchor into one basic model. We denote it as model 4. to analyze the tooth structure, we apply a well-known technique: we place all the ampere-conductors in a uniform layer on the armature surface in the working air gap with an equivalent linear current load. The value of the induction in the gap for this model will be considered equivalent to the real induction. If this assumption is accepted, all analytical expressions, including the electromagnetic moment, electromagnetic power, and model efficiency coefficients, will be similar to the expressions for model 3.

The average electromagnetic torque and electromagnetic power for $(180-180/m)$ -degree commutation on the basis of the above

$$\begin{aligned} M_{srmod4(180-\frac{180}{m})} &= M_{\max mod4(180-\frac{180}{m})} K_{ef(180-\frac{180}{m})} \\ &= \frac{\pi}{2} A_{sr} B_{\delta} D_{sr}^2 L_{ring} K_{mod4(180-\frac{180}{m})} K_{ef(180-\frac{180}{m})}; \end{aligned} \quad (70)$$

$$P_{elmod4(180-\frac{180}{m})} = \frac{\pi}{2} A_{sr} B_{\delta} \omega D_{sr}^2 L_{ring} K_{mod4(180-\frac{180}{m})} K_{ef(180-\frac{180}{m})}. \quad (71)$$

where $K_{mod4(180-\frac{180}{m})}$ – the efficiency coefficient of the model, determined by **Figure 25**.

The average electromagnetic torque and electromagnetic power for 180-degree commutation

$$M_{srmod4(180)} = M_{\max mod4(180)} K_{ef(180)} = \frac{\pi}{2} A_{sr} B_{\delta} D_{sr}^2 L_{ring} K_{mod4(180)} K_{ef(180)}; \quad (72)$$

$$P_{elmod4(180)} = \frac{\pi}{2} A_{sr} B_{\delta} \omega D_{sr}^2 L_{ring} K_{mod4(180)} K_{ef(180)}. \quad (73)$$

where $K_{mod4(180)}$ – the efficiency coefficient of the model, determined by **Figure 26**.

It should be noted that, despite the analogy with model 3, the value of the average electromagnetic power and electromagnetic moment for model 4 would be approximately 4–6 times higher due to higher values of electromagnetic loads (induction in the gap and linear current load on the average armature diameter).

3.6 Comparative analysis of structures at $(180-180/m)$ - degree commutation and 180-degree commutation

This analysis allows us to make a qualitative assessment of the effectiveness of models in terms of the development of the electromagnetic moment in the same volumes. Prong models are more efficient than models with a smooth anchor due to the large values of electromagnetic loads. For a BMAMF with a smooth anchor, due to different values of the model coefficient, we can conclude: model 2 is more efficient than model 1 and model 3 is more efficient than model 2 and, accordingly, model 1. A quantitative analysis of this efficiency is of Practical interest.

We perform this analysis using the following method: for a fixed number of phases, we determine the ratio of electromagnetic powers for different models and different switching options. For a BMAMF with a smooth armature, the value of the electromagnetic loads will be considered the same. The air gap induction value for the toothed armature is approximately 1.6 times higher than the gap induction value for the model 3 smooth armature (80% of the residual permanent magnet induction for the toothed armature and 50% for the smooth armature). Approximately the same ratio can be assumed for linear loads. These relations are confirmed by practical tests. Therefore, for a comparative analysis for model 4, you can enter an increasing coefficient of 2.56 compared to model 3. The Results are summarized in the table.

Table 1 shows a comparison of models for the variant: pole arc coefficient 0.8, number of phases 3, 120-degree commutation.

Table 2 shows a comparison of models for the variant: pole arc coefficient 0.8, number of phases 3, 180-degree commutation.

Tables 1 and 2 show that model 4 is the most efficient in terms of the electromagnetic moment and electromagnetic power.

These tables are convenient to use in practice for choosing the design and type of switching depending on the project.

Comparison of 3-phase models for 120-degree commutation and the pole arc coefficient 0.8		The model to compare with			
		Model 1 	Model 2 	Model 3 	Model 4 
Model for comparison	Model 1 	1	0.577	0.288	0.113
	Model 2 	1.733	1	0.5	0.195
	Model 3 	3.466	2	1	0.391
	Model 4 	8.87	5.12	2.56	1

Table 1.
 Comparison of the efficiency of models based on the developed electromagnetic moment for 120-degree switching.

Comparison of 3-phase models for 180-degree commutation and the pole arc coefficient 0.8		The model to compare with			
		Model 1 	Model 1 	Model 1 	Model 1 
Model for comparison	Model 1 	1	0.667	0.333	0.13
	Model 1 	1.499	1	0.5	0.195
	Model 1 	3.0	2	1	0.391
	Model 1 	7.68	5.12	2.56	1

Table 2.
 A similar comparison for 180-degree commutation.

4. Conclusion

BMAMP is a new class of electric machines. Their use is expanding for electric drives for General industrial applications and special applications in medicine, space and robotics. The theory of their analysis is not fully developed. These studies expand the possibilities of this analysis. The following main conclusions can be drawn from the presented research.

1. Classification of the main types of commutations is carried out. For a BMAMP with an arbitrary number of phases the discrete (180–180/m)-degree commutation and 180-degree commutation with galvanically isolated phase supply are selected.
2. The efficiency factor of the armature winding for various types of commutations is given. It is convenient to use this factor to compare the efficiency of commutation types.
3. The influence of the number of phases on the developed electromagnetic moment for (180–180/m)-degree switching and 180-degree switching is analyzed. It is proved that to increase the electromagnetic moment in the same dimensions and with the same electromagnetic loads, it is necessary to increase the number of phases and the pole arc coefficient for both types of commutation.
4. Classification of BMAMF designs based on the shape of permanent magnets and armature winding sections is carried out. Basic models for analysis are defined.
5. The resulting equation of the electromagnetic torque and electromagnetic power for base structures is given. The equations determine the dependence of energy indicators on the main dimensions, electromagnetic loads, design features, and type of commutation. Model efficiency factors are derived for all basic models.
6. The comparative analysis of the effectiveness of the basic models for electromagnetic power for the same dimensions and the same electromagnetic loads is carried out. The results of the analysis are summarized in tables for different types of switching and the number of phases, quantitatively showing the advantages of one design over another. Tables are convenient to use in engineering practice to select the best option depending on the project situation.

Further research will be aimed at developing methods for computer-aided design of machines of this class.

Author details

Sergey Gandzha* and Dmitry Gandzha
South Ural State University, Chelyabinsk, Russia

*Address all correspondence to: gandzhasa@susu.ru

IntechOpen

© 2021 The Author(s). Licensee IntechOpen. This chapter is distributed under the terms of the Creative Commons Attribution License (<http://creativecommons.org/licenses/by/3.0>), which permits unrestricted use, distribution, and reproduction in any medium, provided the original work is properly cited. 

References

- [1] Gandzha, S.A Application of the Ansys Electronics Desktop Software Package for Analysis of Claw-Pole Synchronous Motor / S.A. Gandzha, B.I. Kosimov, D.S. Aminov //Machines.– 2019.–Vol. 7 No. 4 <https://ieeexplore.ieee.org/document/8570132> DOI: 10.1109/GloSIC.2018.8570132
- [2] Gandzha, S. Selecting Optimal Design of Electric Motor of Pilgrim Mill Drive for Manufacturing Techniques Seamless Pipe / S. Gandzha, B. Kosimov, D. Aminov //2019 International Conference on Industrial Engineering, Applications and Manufacturing, ICIEAM 2019.–2019 <https://ieeexplore.ieee.org/document/8742941> DOI: 10.1109/ICIEAM.2019.8742941
- [3] I.E. Kiessh, S.A. Gandzha, “Application of Brushless Machines with Combine Excitation for a Small and Medium Power Windmills”, *Procedia Engineering*.– 2016.–Vol. 129.– P.191–194, DOI: 10.1016/j.proeng.2016.12.031 <https://www.sciencedirect.com/science/article/pii/S1877705815039156?via%3Dihub>
- [4] Gandzha, S., Andrey, S., Andrey, M., Kiessh, I. The design of the low-speed brushless motor for the winch which operates in sea-water. *International Multidisciplinary Scientific GeoConference Surveying Geology and Mining Ecology Management, SGEM*
- [5] Gandzha, S. The application of the double-fed alternator for the solving of the wind power problems. *International Multidisciplinary Scientific GeoConference Surveying Geology and Mining Ecology Management, SGEM*
- [6] Gandzha S.A., Sogrin A.I., Kiessh I.E. The Comparative Analysis of Permanent Magnet Electric Machines with Integer and Fractional Number of Slots per Pole and Phase. *Procedia Engineering* 129: 408–414, December 2015.
- [7] Gandzha S., Aminov D., Bakhtiyor K. Application of the combined excitation submersible hydrogenerator as an alternative energy source for small and medium rivers. *IEEE Russian Workshop on Power Engineering and Automation of Metallurgy Industry*. 4–5 Oct. 2019 Magnitogorsk, Russia. DOI: 10.1109 / PEAMI.2019.8915294
- [8] Aydin, M. S. Huang and T. A. Lipo. “Axial Flux Permanent Magnet Disc Machines: A Review”, In *Conf. Record of SPEEDAM*, , May 2004, pp. 61–71
- [9] Akatsu K. and Wakui S. “A comparison between axial and radial flux PM motor by optimum design method from the required NTcharacteristics”, *Conference Proceeding of ICEM2004*, No. 361, Cracow-Poland, 2004.
- [10] Gandzha, S., Kiessh, I. The high-speed axial gap electric alternator is the best solution for a gas turbine engine. The high-speed axial gap electric alternator is the best solution for a gas turbine engine. *International Multidisciplinary Scientific GeoConference Surveying Geology and Mining Ecology Management, SGEM*.
- [11] Gandzha, S. Development of engineering technique for calculating magnet systems with permanent magnets / S. Gandzha, E. Kiessh, D.S. Aminov //Proceedings - 2018 International Conference on Industrial Engineering, Applications and Manufacturing, ICIEAM 2018.–2018 No. 10.15593/2224-9397/2019.1.04 <https://ieeexplore.ieee.org/document/8728650> DOI:10.1109/ICIEAM.2018.8728650
- [12] Gandzha S., Bakhtiyor K., Aminov D. Development of a system of multi-level optimization for Brushless Direct Current Electric Machines. *International Ural Conference on Electrical Power Engineering (Ural*

Con) 2019. 1–3 Oct. 2019 Chelyabinsk, Russia. DOI: 10.1109/URALCON.2019.8877650

[13] Gandzha, S., Kiessh, I. Selection of winding commutation for axial gap machines with any phases. Proceedings - 2018 International Conference on Industrial Engineering, Applications and Manufacturing, ICIEAM 2018

[14] Gandzha S.A. Application of Digital Twins Technology for Analysis of Brushless Electric Machines with Axial Magnetic Flux / Gandzha, S. // Proceedings - 2018 Global Smart Industry Conference, GloSIC 2018.– 2018 <https://ieeexplore.ieee.org/document/8570132> DOI:10.1109/GloSIC.2018.8570132

[15] Gandzha, S. Design of Brushless Electric Machine with Axial Magnetic Flux Based on the Use of Nomograms / S. Gandzha, D. Aminov, B. Kosimov // Proceedings - 2018 International Ural Conference on Green Energy, UralCon 2018.–2018.– P.282–287 <https://ieeexplore.ieee.org/document/8544320> DOI: 10.1109/URALCON.2018.8544320